ADVANCED FUNCTIONAL MATERIALS
www.afm-journal.de

www.MaterialsViews.com

N-Type Self-Assembled Monolayer Field-Effect Transistors and Complementary Inverters

Andreas Ringk, Xiaoran Li, Fatemeh Gholamrezaie, Edsger C. P. Smits, Alfred Neuhold, Armin Moser, Cees Van der Marel, Gerwin H. Gelinck, Roland Resel, Dago M. de Leeuw, and Peter Strohriegl**

This work describes n-type self-assembled monolayer field-effect transistors (SAMFETs) based on a perylene derivative which is covalently fixed to an aluminum oxide dielectric via a phosphonic acid linker. N-type SAMFETs spontaneously formed by a single layer of active molecules are demonstrated for transistor channel length up to 100 μm. Highly reproducible transistors with electron mobilities of 1.5×10^{-3} cm^2 V^{-1} s^{-1} and on/off current ratios up to 10^5 are obtained. By implementing n-type and p-type transistors in one device, a complimentary inverter based solely on SAMFETs is demonstrated for the first time.

1. Introduction

Self-assembled monolayers (SAMs) are dense organic layers spontaneously formed on a surface.[1] The autonomous and selective organization of molecules without human intervention is a promising technology for mass production of organic electronics. Self-assembled monolayer field-effect transistors (SAMFETs) where the organic semiconductor consists of only one monolayer covalently anchored onto the dielectric have been reported.[2,3] The covalent fixation of the active material to the dielectric allows the fabrication of flexible and transparent devices[4] with reduced delamination of the semiconductor during bending. The absence of bulk material eliminates bulk currents to give high on/off current ratios. Recent publications have shown that truly two dimensional semiconducting systems are exhibiting confinements effects with new charge transport[5] and are well suitable for analyzing charge transport without interferences from the bulk.[6,7] A dense packing of the chromophores, full coverage, and strong π–π coupling over long distances are required for reliable devices[8] and enable a two dimensional charge transport between the source and drain electrodes.

So far the most promising SAMFETs have been demonstrated using a quinquethiophene derivative attached to silicon dioxide.[9] Hole mobilities up to 10^{-2} cm^2 V^{-1} s^{-1} were achieved and the first unipolar integrated circuits as for example a 15-bit code generator based on SAMFETs, were made. State of the art integrated circuits however are mostly based on the well-established complementary metal oxide semiconductor (CMOS) technique, where pairs of p- and n-type transistors are combined in one device. This circuit design results in high noise immunity and low power consumption. To realize complementary organic circuits based on self-assembled monolayers, suitable n-type materials for the preparation of SAMFETs are required. Compared to p-type materials it is difficult to find n-type transistor materials, because of their high reactivity towards oxygen and moisture.[10,11] Only recently have stable n-type semiconducting materials been demonstrated with mobilities matching those of p-type semiconductors.[12,13]

Progress on fabricating n-type SAMFETs has been reported.[14] A semiconducting fullerene based monolayer

A. Ringk, Prof. P. Strohriegl
Macromolecular Chemistry I
University of Bayreuth
95440 Bayreuth, Germany
E-mail: Peter.Strohriegl@uni-bayreuth.de
A. Ringk, F. Gholamrezaie
Dutch Polymer Institute (DPI)
P.O. Box 902, 5600 AX Eindhoven, The Netherlands
X. Li, Dr. E. C. P. Smits, Dr. G. H. Gelinck
Holst Centre/TNO
High Tech Campus 31, 5656 AE Eindhoven, The Netherlands
E-mail: Edsger.Smits@tno.nl
X. Li
Department of Chemical Engineering and Chemistry
Eindhoven University of Technology
P.O. Box 513, 5600 MB Eindhoven, The Netherlands
F. Gholamrezaie, D. M. de Leeuw
Philips Research Laboratories
High Tech Campus 4,
5656 AE Eindhoven, The Netherlands
Molecular Electronics
Zernike Institute for Advanced Materials
University of Groningen
Nijenborgh 4, 9747 AG Groningen, The Netherlands
A. Neuhold, A. Moser, R. Resel
Institute of Solid State Physics
Graz University of Technology
Petersgasse 16, A-8010 Graz, Austria
C. van der Marel
Philips Innovation Services–Materials Analysis
High Tech Campus 11, 5656 AE Eindhoven, The Netherlands

DOI: 10.1002/adfm.201202888

(C60C18-PA) on aluminum oxide was shown to exhibit electron mobilities up to 10^{-4} cm^2 V^{-1} s^{-1}. A major issue in this work is that the C60C18-PA monolayers tend to form disordered layers with poor electrical properties as a result. A possible suggested solution is to use mixed monolayers. By the combination of C60C18-PA together with a C12 fluorinated phosphonic acid the out of plane order in the SAMs could be improved. The result–a mixed monolayer of both species–will however always be a necessary trade-off between interfacial order and surface coverage.[15] The lack of reliable n-type SAMFET materials hampers the realization of self-assembled CMOS circuits. High performance and reliable n-type SAMFETs will enable a huge step forward in a bottom-up approach towards robust self-assembled complementary organic circuits.

Here we present reproducible n-type SAMFETs based on heterosubstituted perylene bisimides with mobilities up to 1.5×10^{-3} cm^2 V^{-1} s^{-1}. By implementing p- and n-type transistors, a complementary inverter based solely on SAMFETs with large noise margin of 7 V and a gain up to 15 are demonstrated.

2. Results and Discussion

2.1. SAMFET Device Preparation

The perylene bisimide derivative N-(1-hexylheptyl)-N′-(undecyl-11-phosphonic acid) perylene-3,4,9,10-tetracarboxylic bisimide, (PBI-PA), was synthesized as the n-type active material in our SAMFETs. The molecule belongs to a class of semiconductors well-known for their high performance in n-type organic transistors.[11] The chemical structure of PBI-PA is shown in **Figure 1**. The active molecule PBI-PA consists of a heterosubstituted perylene bisimide core bearing a branched alkyl tail to increase the solubility on one side, and a linear undecyl alkyl chain with a phosphonic acid anchor group on the other side. The phosphonic acid allows a covalent fixation of PBI-PA to aluminum oxide. Major benefits of phosphonic acid terminated molecules compared to the chlorosilanes previously reported[9] are easier handling, storage and device fabrication as they are environmentally stable.

The substrates for the SAMFET preparation consist of a silicon monitor wafer with patterned gold gate electrodes on which a 100-nm-thick aluminum oxide layer is deposited by atomic layer deposition (ALD). Gold source and drain electrodes and vertical interconnections are made by conventional photolithography.[16] To facilitate the anchoring of the phosphonic acid to the dielectric, the substrate was cleaned with acetone and isopropanol and activated by UV-ozone treatment.

A high tendency to form aggregates in solution is well known for perylene bisimides. However, the formation of large aggregates is undesirable for depositing smooth and dense monolayers on surfaces. Spectroscopic investigations revealed that at low concentrations of about 10^{-5} M, aggregation of perylenes is suppressed.[17] Therefore bottom-gate/bottom-contact PBI-PA SAMFETs were prepared by immersing the transistor substrate into a dilute solution of PBI-PA in tetrahydrofuran (1.5×10^{-5} M). During the immersion the phosphonic acid reacts in a condensation reaction with the OH-groups on the oxide surface to form a covalent bond.[18] In comparison to thiols, which form relatively weak bonds to gold, phosphonic acids bind more strongly to aluminum oxide.[19]

After immersion for 24 h under ambient atmosphere and room temperature, the devices were dipped into tetrahydrofuran and annealed at 120 °C under N_2 atmosphere for 20 min. Subsequently the SAMFETs were analyzed and measured.

2.2. Monolayer Analysis

To characterize the SAMs, atomic force microscopy (AFM), X-ray photoelectron spectroscopy (XPS), X-ray reflectivity (XRR), and grazing incidence X-ray diffraction (GIXD) investigations were carried out. AFM measurements revealed a smooth and uniform surface, typical for a monolayer (**Figure 2**). The apparent lack of structures confirms the presence of a smooth

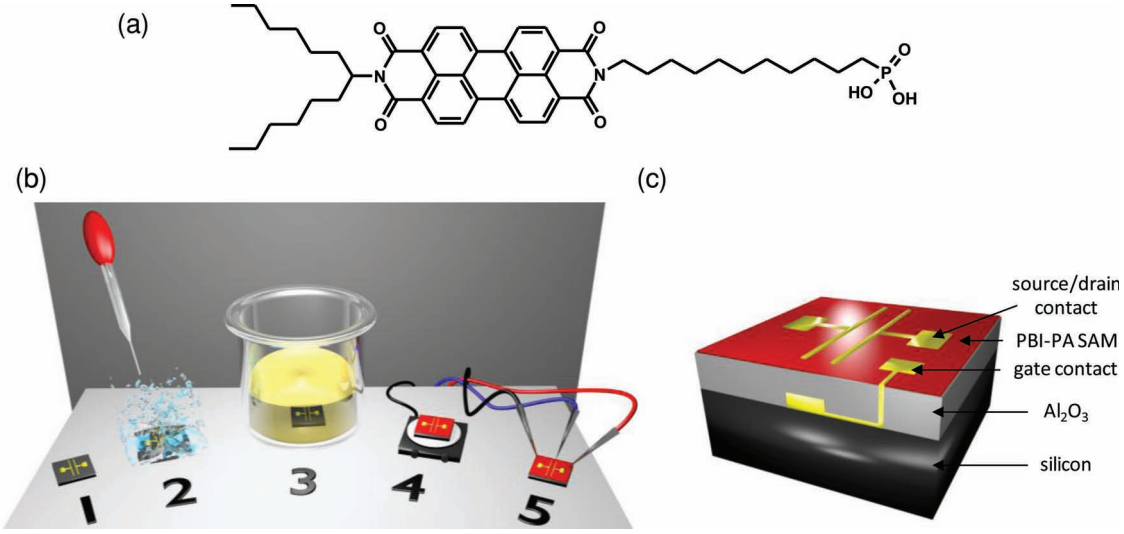

Figure 1. a) Chemical structure of PBI-PA. b) Illustration of the n-type SAMFET fabrication process. c) Scheme of SAMFET layout.

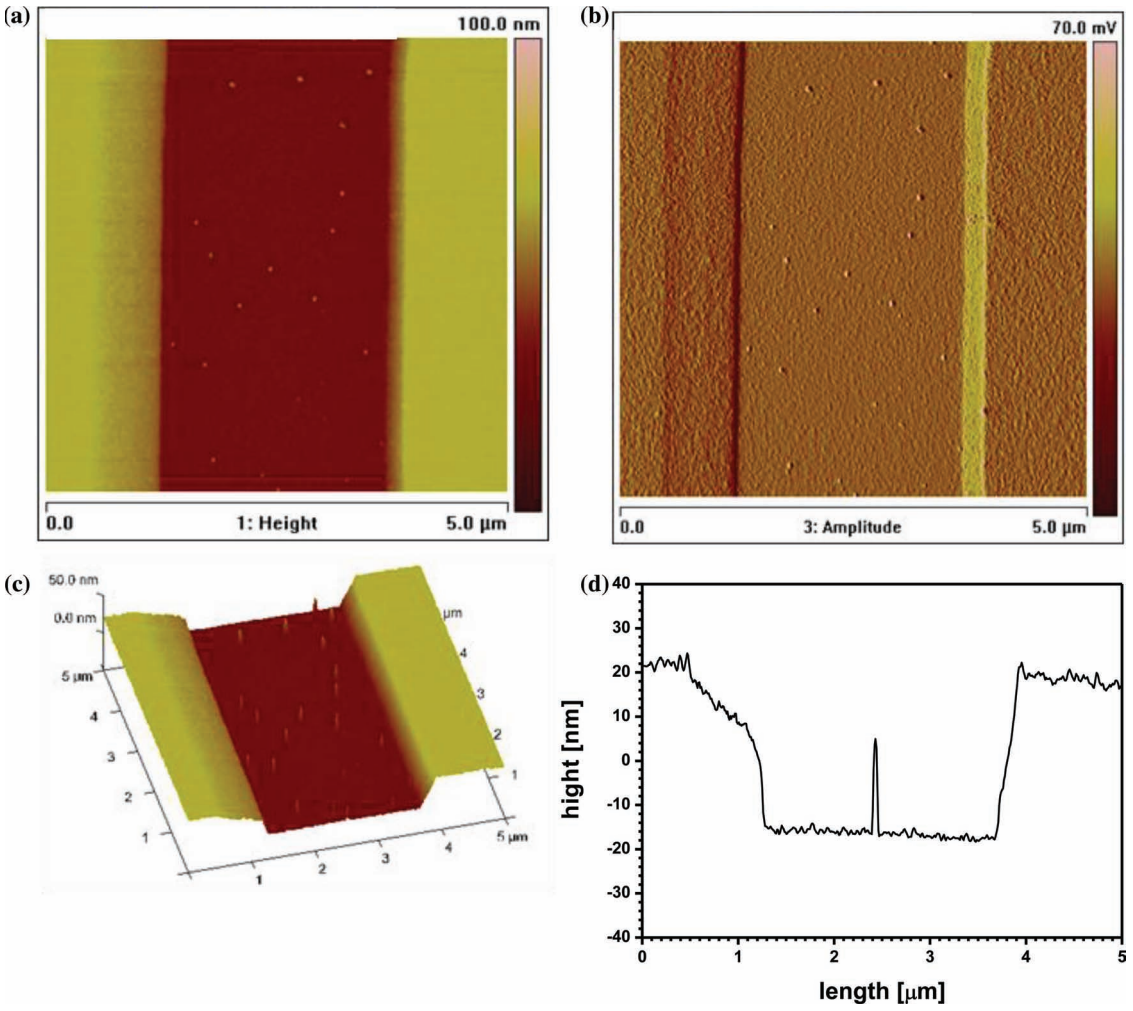

Figure 2. AFM images (5 µm × 5 µm) of a transistor substrate with a PBI-PA monolayer. a) Height image of a transistor channel with a PBI-PA monolayer. b) Phase amplitude image of the transistor channel. c) 3D illustration of panel (a). d) Cross section through the transistor channel.

conformal monolayer similar to other semiconducting monolayers on SiO_2.[9] Only a few particles of 100 nm in diameter are present. Presumably they are aggregates of PBI-PA molecules. As they are so sparsely distributed electrical conduction through the aggregates can be ruled out.

The chemical composition of the same layer was investigated by angle dependent XPS measurements. The results revealed a thin organic layer on the Al_2O_3 surface with an estimated thickness of 3.1 nm ± 0.2 which is in line with the calculated molecular length of 2.9 nm. This confirms the proper formation of the monolayer on the surface. To determine the extent of surface coverage by XPS analysis, phosphorus was chosen as a marker because each molecule has only one phosphorus atom and no other source of phosphorus is present in the system. A number of $1.8 \times 10^{14} \pm 0.2 \times 10^{14}$ phosphorus atoms per cm^2 was measured which corresponds to a complete coverage, estimated by the unit cell dimensions of a known perylene bisimide derivative with branched alkyl tails.[20]

The out of plane order of the pristine PBI-PA SAMs prepared on Al_2O_3 substrates was analyzed by X–ray reflectivity measurements. The experimental data were simulated with a model containing the Al_2O_3 substrate and the monolayer separated into three layers with different thicknesses, r.m.s roughness and densities (**Table 1**). The bottom layer of the SAM is formed by the spacer and anchor groups of the molecule, the middle layer consists of the aromatic cores and the top layer is assembled by the terminal alkyl group of the molecule. Alternatively, a two layer fitting model and a fitting model comprising the SAM as a single layer with constant density were performed (not shown). However, the three layer model presented here gives the physically most realistic description of the measured XRR data. **Figure 3** illustrates the different separated parts of the SAM used in the fitting model and the experimental XRR data (black line) with the associated fit (red line). The thicknesses of the end group layer, the aromatic core layer and the spacer with anchor group layer are found to be 0.71, 0.98, and 1.32 nm, respectively. The numbers are in good agreement with the estimated lengths of the individual molecular units which were found to be 0.63, 1.13, and 1.17 nm by molecular modeling. The numerical fit reveals that the density

Table 1. Layer thickness d, r.m.s. roughness σ, mass density, ρ_m, and electron density ρ_{el} of the individual parts of the investigated PBI-PA SAM on the Al_2O_3 substrate extracted from the XRR data shown in Figure 3.

Layer	d [nm]	σ [nm]	ρ_m [g/cm^3]	ρ_{el} [nm^{-3}]
alkyl groups	0.71 ± 0.05	0.28 ± 0.05	0.48 ± 0.07	157 ± 5
aromatic core	0.98 ± 0.06	0.45 ± 0.05	1.23 ± 0.02	391 ± 6
spacer with anchor group	1.32 ± 0.10	0.12 ± 0.03	0.81 ± 0.03	259 ± 4
Al_2O_3 substrate	165.23 ± 4.31	0.85 ± 0.08	2.89 ± 0.10	862 ± 6

of the middle layer is considerably enhanced in comparison with the other two layers, which supports the presence of aromatic carbon, nitrogen and oxygen. In the XRR simulation the anchor group was coupled with the spacer group and due to the presence of phosphor and oxygen the density is increased, compared to the density of the top alkyl group. Next to the molecular parameters, the XRR graph additionally comprises the substrate information. The rapid oscillations in the graph originate from the 165-nm-thick Al_2O_3 layer (Table 1), of the plain Al_2O_3 substrates, which is emphasized in the insert of Figure 3.

The XPS, AFM, and XRR measurements show that PBI-PA forms a densely packed monolayer. To investigate the in-plane order we performed grazing incidence X-ray diffraction measurements. Due to the absence of periodicity perpendicular to the SAM layer, any long-range in-plane order is manifested as Bragg rods. A typical example is chloro[11-(5′′′′-ethyl-2,2′:5′,2′′:5′′,2′′′:5′′′,2′′′′-quinquethien-5-yl)undecyl]dimethylsilane self-assembled on SiO_2.[9] The diffracted intensity as a function of in-plane scattering vector, q_{xy}, is presented in **Figure 4**. Bragg rods are not found. Only a broad diffraction peak (q_{xy}) at 17.5 nm^{-1} corresponding to an intermolecular distance of 0.36 nm is observed. From the width of the diffraction peak (Δq_{xy}) of 2 nm^{-1}, the correlation length, or crystal

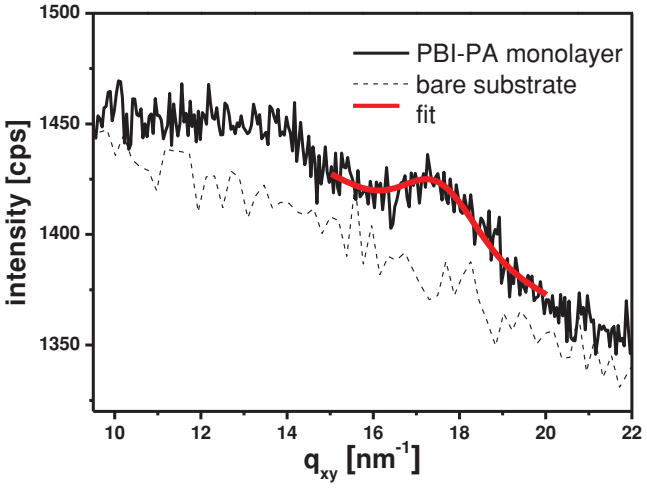

Figure 4. Grazing incidence X-ray diffraction (GIXD) of a PBI-PA monolayer together with the scattering signal of the bare aluminum oxide substrate. The intensity was measured with a one-dimensional detector and integrated in the q_z range between 0 and 3 nm^{-1}. A Gaussian fitting curve to the peak at 17.5 nm^{-1} is plotted in red color.

size, was estimated to be 3.1 nm. The extracted length corresponds to only 9 repeated conjugated units. The PBI-PA SAM forms a nano-crystalline layer. We note that the weak crystallinity can be inferred from X-ray diffraction studies on bulk branched perylene derivatives.[20–22] The packing of alkyl terminated PBI-PA based molecules is dominated by the interaction between the conjugated PBI-PA cores. The π–π stacking of the aromatic cores leads to parallel stacks with a typical distance of 0.36 nm.[23–25] where the aromatic chains are arranged perpendicular to the substrate surface. However, the stacks arrange themselves in twisted columns without long range order. The nano-crystallinity along the columns is confirmed by XRD measurement on bulk PBI-PA material, which also shows a very broad diffraction peak at the same distance (Supporting

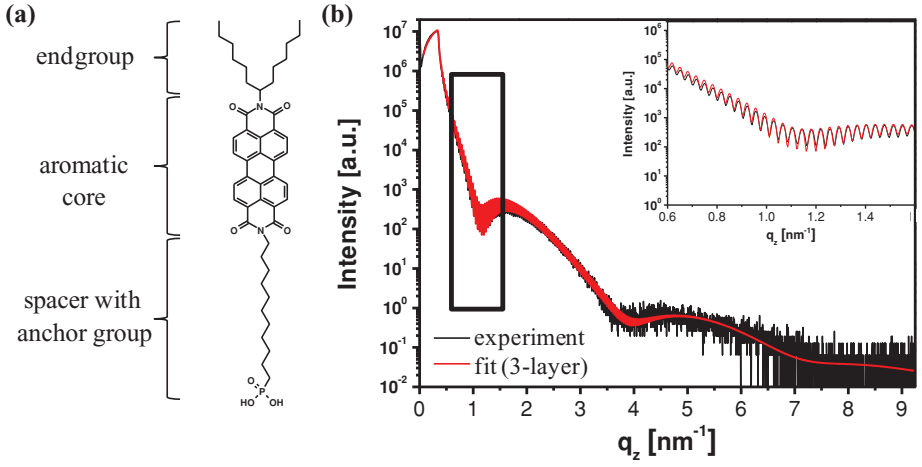

Figure 3. X-ray reflectivity (XRR) investigation of PBI-PA monolayers. a) The sketch shows the three separated molecule parts, which were used for the XRR simulation. b) The graph illustrates the XRR of the PBI-PA monolayer on aluminum oxide. The red solid line gives the simulation to the experimental data (black line). The insert of the graph illustrates the thickness oscillations of the Al_2O_3 substrate around the first minimum.

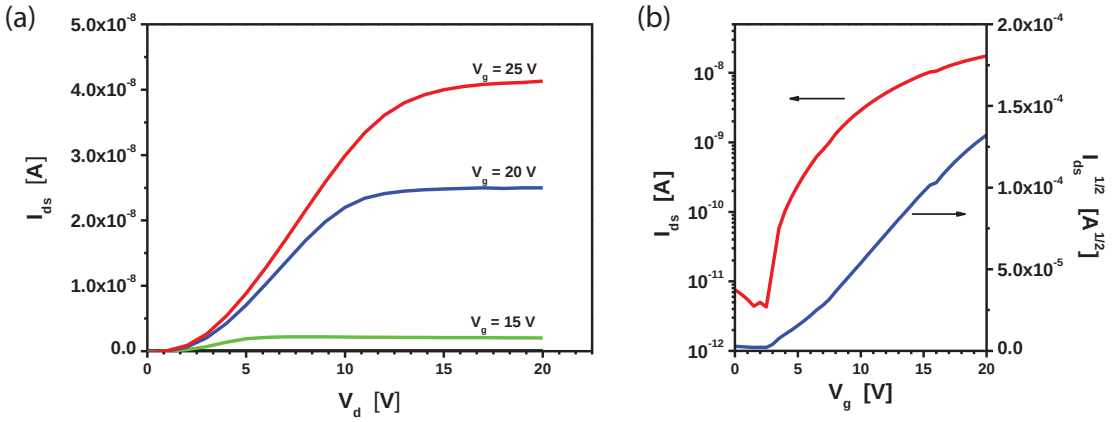

Figure 5. Transistor measurements of PBI-PA SAMFETs. a) Output characteristics of a SAMFET having a channel length of 40 µm and a channel width of 1000 µm. The drain voltage is swept from 0 to 20 V, the gate voltage is varied starting from 0 to 25 V in 5 V per step. b) Transfer characteristics of the same device in the saturation regime with a drain voltage of 20 V.

Information Figure S2). The interplay between steric repulsion of branched alkyl tails, π–π packing effects, and self-assembly of the phosphonic acid groups ultimately results in nano-crystalline self-assembled monolayers of PBI-PA.[24]

2.3. Electrical Characterization

The output and transfer characteristics of an n-type PBI-PA SAMFET with a channel length of 40 µm and a channel width of 1000 µm are shown in **Figure 5**a,b.

The saturation mobility of the transistor is 1.5 × 10^{-3} cm^2 V^{-1} s^{-1}, with an on/off-current ratio on the order of 10^4 and a threshold voltage close to zero. We note that properly functioning device characteristics were obtained for short as well as long channel length devices up to 100 µm, for the first time.[14,15] Field-effect behavior was obtained for all measured transistors, i.e., device yield of 100%, which is indicative of a high reproducibility over large areas. The transistors were contact limited as confirmed by the nonlinear "s" shaped behaviour at the low drain bias in the output characteristics (Figure 5a). We have used Au source and drain electrodes with a work function of ≈5 eV. The LUMO of the PBI-PA is estimated at around 3.8 eV.[26] Despite the injection barrier of more than 1 eV, electrons can still be injected. Comparable contact limited injection has been reported for thin-film transistors of semiconducting PBI derivatives.[27]

The saturation mobility as a function of channel length is presented in **Figure 6**. In short channel transistors the transport is limited by the contact resistance which lowers the mobility.[28] For long channels the mobility is constant up to a channel length of 100 µm. The constant mobility is remarkable. Traditionally, as reported previously for p-type SAMFETs,[8] the mobility of self-assembled monolayer field-effect transistors decreases dramatically with increasing channel length. This dependence is a direct consequence of incomplete coverage. Here the mobility remains constant for channel lengths up to 100 µm, which is a fingerprint of complete coverage with long-range connectivity within the SAM. The constant mobility for long channel length, as shown in Figure 6, reflects the homogeneous long-range charge transport through a densely packed monolayer without conduction barriers from, for example, grain boundaries or from incomplete coverage. The channel-length dependence of the carrier mobility, XPS investigations, XRR, and XRD data confirm that a fully covered and conductive self-assembled monolayer of PBI-PA was formed on the aluminum oxide surface.

A crucial step towards realizing robust and low power circuits is the use of complementary logic. For SAMFET based complementary circuits reliable n-type as well as p-type SAMFETs are essential. For this purpose p-type and n-type SAMFETs were fabricated on two substrates and connected in a complementary inverter configuration. The p-type transistors were fabricated as described previously,[9] and consist of a quinquethiophene derivative grafted to a silicon dioxide dielectric via a dimethylchlorosilane anchor group. As the n-type material PBI-PA anchored to an aluminum oxide dielectric a phosphonic acid group was taken. Due to the difference in mobility, the currents

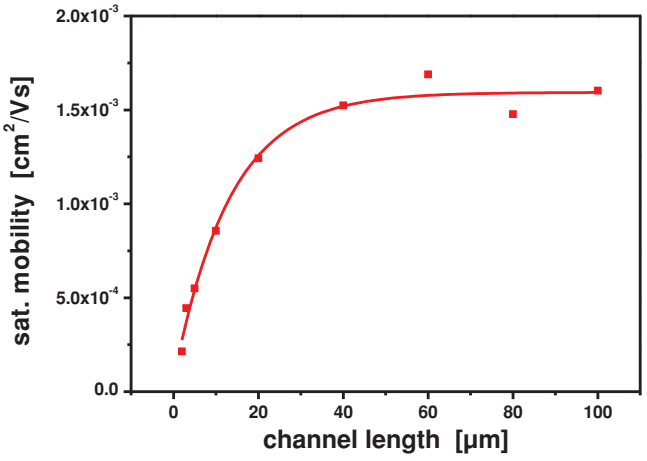

Figure 6. Scaling of mobility. The saturation mobility of PBI-PA SAMFETs as a function of channel length (ranging from 2 to 100 µm). For channel lengths smaller than 40 µm the mobility is dominated by the contact resistance. For larger channels the mobility becomes independent of the channel length. The red line is a guide for the eye.

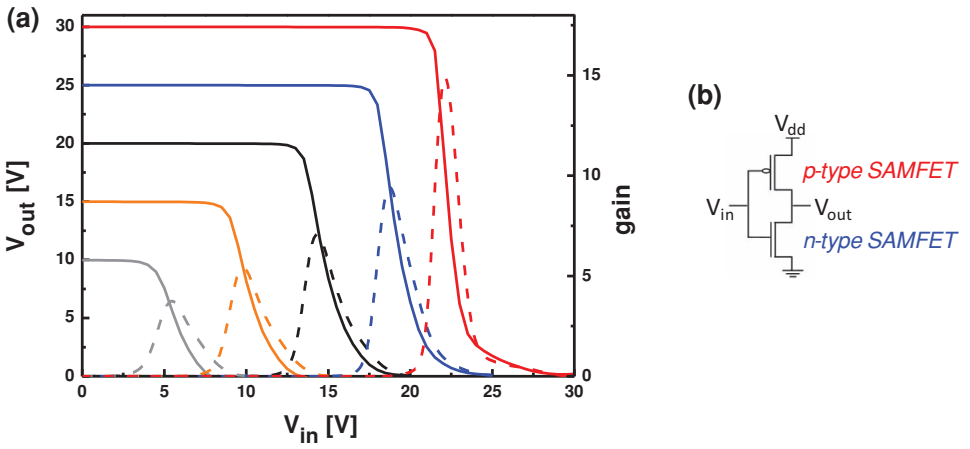

Figure 7. SAMFET based complementary inverter. a) Device characteristics: The supply voltage (V_{dd}) was varied starting from 10 to 30 V in 5 V per step. The dashed lines present the gains. b) Diagram of the SAMFET CMOS inverter.

from both transistors were matched by adjusting the channel length. For the p-type SAMFET a channel length of 40 µm was chosen and a 2 µm channel length was taken for the n-type SAMFET. Both transistors had a channel width of 1000 µm. Prior electrical measurements confirmed that both SAMFETs showed a proper conductivity typical for dense organic monolayers on top of oxides. The resulting inverter characteristics are shown in **Figure 7**. When the supply voltage (V_{dd}) was set at 30 V and the input voltage (V_{in}) was swept from 30 to 0 V with a typical scan speed of 1 V s^{-1} (red curve in Figure 7a), a high gain value of ≈15 with the "trip-point" at around 23 V of V_{in} was obtained. Here, gain is defined as dV_{out}/dV_{in}. The so-called "maximal equal criterion" noise margin[29] of 7 V (for V_{dd} = 30 V) was substantially larger than values reported for PMOS inverters used in complex circuitry,[29,30] also higher than the previous unipolar p-type SAMFET inverters (Supporting Information Figure S10a), and on par with conventional organic CMOS.[29]

3. Conclusion

In summary, we present n-type SAMFETs based on a perylene derivative with a phosphonic acid anchor group which enables an efficient fixation to aluminum oxide. Simple device fabrication under ambient conditions leads to a complete surface coverage of the monolayer and to transistors with electron mobilities up to 10^{-3} cm^2 V^{-1} s^{-1} for channel length as long as 100 µm. By implementing p- and n-type SAMFETs in one circuit, a complementary inverter based solely on SAMFETs with a large noise margin and a high gain is demonstrated for the first time, paving the way to robust and low power self-assembled monolayer based complementary circuits.

4. Experimental Section

Further information on molecular modeling, atomic force microscopy (AFM), X-ray diffraction studies, transistor substrate manufacture, and electrical characterization are given in the Supporting Information.

An overview of the synthesis towards PBI-PA is shown in **Figure 8**.

Synthesis of PBI-PA 6 N-(1-hexylheptyl)-N′-(undecyl-11-phosphonic Acid) Perylene-3,4,9,10-tetracarboxylic Bisimide: The starting materials perylene-3,4,9,10-tetracarboxylic-3,4,9,10-dianhydride, potassium hydroxide, ammonia, 1,11-dibromoundecane, sodium hydride, triethyl phosphite, bromotrimethylsilane, and solvents were purchased from Aldrich, Acros Organics and VWR. Solvents used for precipitation and column chromatography were distilled once before use. ^{1}H- and ^{13}C-NMR spectra were recorded on a Bruker AC 250 spectrometer (250 MHz). Chemical shifts are reported in ppm at room temperature using $CDCl_3$ as solvent and internal standard. Mass spectroscopic data were obtained from a FINNIGAN MAT 8500 instrument.

Synthesis of N-(1-hexylheptyl)-N′-(undecylbromide) Perylene-3,4,9,10-tetracarboxylic Bisimide 4: Perylenebisimide 3 (530 mg, 0.93 mmol) and sodium hydride (46 mg, 65% dispersed in mineral oil, 1.24 mmol) were dissolved in 45 mL dry DMF and stirred at room temperature. After 24 h the solution was heated to 90 °C and 1,11-dibromoundecane (5 g, 15.9 mmol) were added. After 60 h the reaction mixture was poured into water and extracted with $CHCl_3$. The solvent was evaporated, the crude product redissolved in $CHCl_3$ and poured into hexane. The precipitate was filtered off and purified by flash chromatography (solvent gradient from hexaneto $CHCl_3$). The resulting red solid was freeze dried with dioxane to yield 365 mg (0.453 mmol, 49%) of bromide 4.

TLC ($CHCl_3$): R_f = 0.65. EIMS(*m*/*z*): $[M]^+$ calculated for $C_{48}H_{57}BrN_2O_4$, 805.90 g mol^{-1}; found, 806 g mol^{-1}. ^{1}H-NMR (300 MHz, $CDCl_3$, δ): 0.82 (t, J = 6.9 Hz, 6H; CH_3), 1.20–1.45 (m, 30H; CH_2), 1.70–1.80 (m, 2H; CH_2), 1.80–1.93 (m, 4H; CH_2), 2.18–2.32 (m, 2H; CH_2), 3.36–3.44 (t, J = 3.7 Hz, 2H; CH_2), 4.18 (t, J = 7.6 Hz, 2H; CH_2), 5.13–5.24 (m, 1H; CH), 8.58–8.78 (m, 8H; Ar-H). ^{13}C-NMR (75 MHz, $CDCl_3$, δ): 14.38, 22.93, 27.31, 27.48, 28.54, 29.10, 29.58, 29.67, 29.74, 29.80, 29.81, 30.05, 32.12, 32.76 (alkyl C), 33.22 (C-Br), 34.33 (alkyl C), 41.03, 55.18 (N-C), 123.29, 123.39, 123.60, 126.69, 126.80, 129.70, 129.89, 131.68, 134.97, 163.67 (aromatic C).

Synthesis of N-(1-hexylheptyl)-N′-(undecylphosphonic acid diethylester) Perylene-3,4,9,10-tetracarboxylic Bisimide 5: Perylenebisimide 4 (759 mg, 0.942 mmol) was dissolved in 200 mL triethyl phosphite and heated to 150 °C for 24 h. The excess of triethyl phosphite was removed by vacuum distillation and the remaining solid purified by flash chromatography (THF/Hexane 1:1) to yield 800 mg (0.927 mmol, 98%) of 5 as red solid.

TLC (THF: Hexane, 1:1): R_f = 0.5. EIMS(*m*/*z*): $[M]^+$ calculated for $C_{52}H_{67}N_2O_7P$, 863.10 g mol^{-1}; found, 863 g mol^{-1}. ^{1}H-NMR (300 MHz, $CDCl_3$, δ): 0.83 (t, J = 6.7 Hz, 6H; CH_3), 1.20–1.40 (m, 38H; CH_2), 1.51–1.60 (m, 2H; CH_2), 1.73–1.78 (m, 2H; CH_2), 1.80–1.94 (m, 2H; CH_2), 2.18–2.33 (m, 2H; CH_2), 4.03–4.12 (m, 4H; CH_2), 4.14–4.21 (m, 2H),

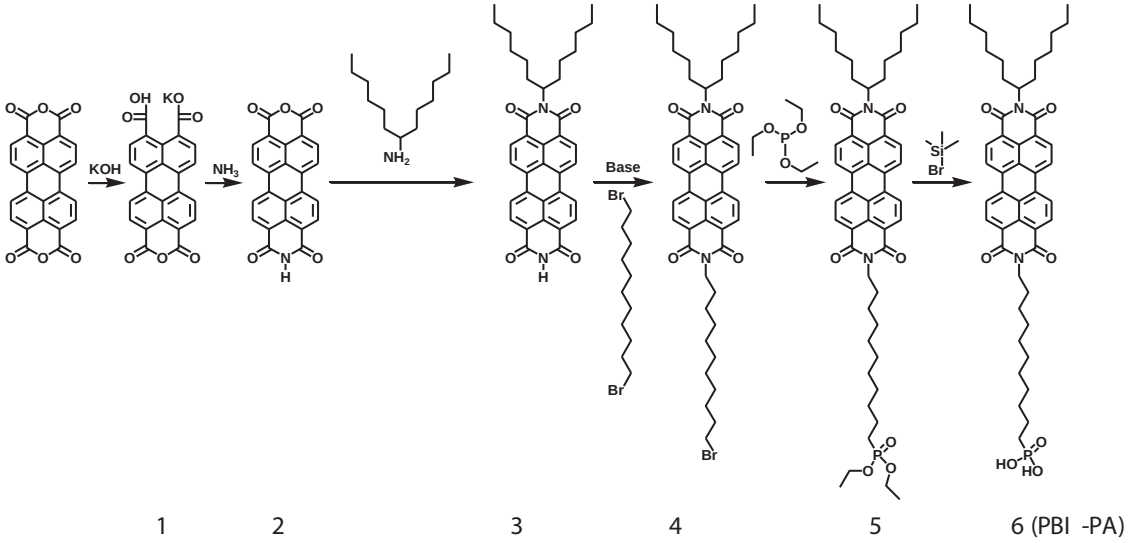

Figure 8. Overview of the synthetic strategy towards the target molecule PBI-PA. Compounds 1–3 were synthesized according to a procedure described in the literature.[31]

5.12–5.24 (m, 1H; CH), 8.43–8.73 (m, 8H; Ar-H). ^{13}C-NMR (75 MHz, $CDCl_3$, δ): 14.20, 22.51, 22.51, 22.58, 22.73, 24.88, 26.74. 27.08, 27.28, 28.24, 29.22, 29.37, 29.50, 29.66, 30.66, 30.89, 31.90, 32.50 (alkyl C), 54.94 (C-N), 61.54 (C-P), 123.08, 123.17, 123.29, 126.39, 126.49, 129.41, 129.63, 131.44, 134.69, 163.44 (aromatic C). ^{31}P-NMR (120 MHz, $CDCl_3$, δ): 32.60.

Synthesis of N-(1-hexylheptyl)-N′-(undecylphosphonic acid) Perylene-3,4,9,10-tetracarboxylic Bisimide 6 (PBI-PA): Perylenebisimide 5 (400 mg, 0.46 mmol) was dissolved under argon in 40 mL dry CH_2Cl_2, cooled to 0 °C and bromotrimethylsilane (1 mL, 7.58 mmol) was added dropwise through a syringe. After addition of the silane, the reaction mixture was allowed to warm up to room temperature. After 48 h stirring, 5 mL water was added. After additional 2 h, the mixture was poured into 50 mL of a mixture of methanol and water (1:1). The resulting precipitate was collected by filtration and freeze dried from dioxane to obtain 352 mg (0.44 mmol, 95%) of the phosphonic acid 6 which was used without further purification.

^{1}H-NMR (300 MHz, $CDCl_3$, δ): 0.79–0.87 (t, J = 6.6 Hz, 6H; CH_3), 1.19–1.49 (m, 34H; CH_2), 1.57–1.65 (2H, m; CH_2), 1.70–1.75 (m, 2H; CH_2), 1.87–1.93 (m, 2H; CH_2), 4.08–4.16 (t, J = 6.4 Hz, 2H; CH_2), 5.09–5.20 (m, 1H; CH_1), 8.24–8.53 (m, 8H; Ar-H).

Supporting Information

Supporting Information is available from the Wiley Online Library or from the author.

Acknowledgements

A.R. and X.L. contributed equally to this work. The work of A.R. and F.G. forms part of the research programme of the Dutch Polymer Institute (DPI), project 624 and 627. We are grateful to Bas van der Putten (Holst Centre) for technical assistance, to Ingo Salzmann (Humboldt University Berlin) for help with the X-ray measurements and the Austrian Science Foundation FWF:[P21094].

Received: October 5, 2012
Published online: November 19, 2012

[1] G. M. Whitesides, *Science* **2002**, *295*, 2418.
[2] G. S. Tulevski, Q. Miao, M. Fukuto, R. Abram, B. Ocko, R. Pindak, M. L. Steigerwald, C. R. Kagan, C. Nuckolls, *J. Am. Chem. Soc.* **2004**, *126*, 15048.
[3] D. O. Hutchins, O. Acton, T. Weidner, N. Cernetic, J. E. Baio, G. Ting, D. G. Castner, H. Ma, A. K.-Y. Jen, *Org. Electron.* **2012**, *13*, 464.
[4] F. Gholamrezaie, S. G. J. Mathijssen, E. C. P. Smits, T. C. T. Geuns, P. A. van Hal, S. A. Ponomarenko, H. G. Flesch, R. Resel, E. Cantatore, P. W. M. Blom, D. M. de Leeuw, *Nano Lett.* **2010**, *10*, 1998.
[5] J. J. Brondijk, W. S. C. Roelofs, S. G. J. Mathijssen, A. Shehu, T. Cramer, F. Biscarini, P. W. M. Blom, D. M. de Leeuw, *Phys. Rev. Lett.* **2012**, *109*, 056601.
[6] W. S. C. Roelofs, S. G. J. Mathijssen, R. A. J. Janssen, D. M. de Leeuw, M. Kemerink, *Phys. Rev. B* **2012**. *8*, 85202.
[7] F. Gholamrezaie, M. Kirkus, S. G. J. Mathijssen, D. M. de Leeuw, S. C. J. Meskers, *J. Phys. Chem. A* **2012**, *29*, 7645.
[8] S. G. J. Mathijssen, E. C. P. Smits, P. A. van Hal, H. J. Wondergem, S. A. Ponomarenko, A. Moser, R. Resel, P. A. Bobbert, M. Kemerink, R. A. J. Janssen, D. M. de Leeuw, *Nat. Nanotechnol.* **2009**, *4*, 674.
[9] E. C. P. Smits, S. G. J. Mathijssen, P. A. van Hal, S. Setayesh, T. C. T. Geuns, K. A. H. A. Mutsaers, E. Cantatore, H. J. Wondergem, O. Werzer, R. Resel, M. Kemerink, S. Kirchmeyer, A. M. Muzafarov, S. A. Ponomarenko, B. de Boer, P. W. M. Blom, D. M. de Leeuw, *Nature* **2008**, *455*, 956.
[10] D. M. de Leeuw, M. M. J. Simenon, A. R. Brown, R. E. F. Einerhand, *Synth. Met.* **1997**, *87*, 53.
[11] B. A. Jones, A. Facchetti, M. R. Wasielewski, T. J. Marks, *J. Am. Chem. Soc.* **2007**, *129*, 15259.
[12] H. Yan, Z. Chen, Y. Zheng, C. Newman, J. R. Quinn, F. Dötz, M. Kastler, A. Facchetti, *Nature* **2009**, *457*, 679.
[13] J. Soeda, T. Uemura, Y. Mizuno, A. Nakao, Y. Nakazawa, A. Facchetti, J. Takeya, *Adv. Mater.* **2011**, *23*, 3681.
[14] M. Novak, A. Ebel, T. Meyer-Friedrichsen, A. Jedaa, B. F. Vieweg, G. Yang, K. Voitchovsky, F. Stellacci, E. Spiecker, A. Hirsch, M. Halik, *Nano Lett.* **2011**, *11*, 156.
[15] A. Rumpel, M. Novak, J. Walter, B. Braunschweig, M. Halik, W. Peukert, *Langmuir* **2011**, *27*, 15016.
[16] A. K. Tripathi, E. C. P Smits, J. B. P. H. van der Putten, M. van Neer, K. Myny, M. Nag, S. Steudel, P. Vicca, K. O'Neill, E. van Veenendaal,

J. Genoe, P. Heremans, G. H. Gelinck, *Appl. Phys. Lett.* **2011**, *98*, 162102.
[17] Z. Chen, V. Stepanenko, V. Dehm, P. Prins, L. D. A. Siebbeles, J. Seibt, P. Marquetand, V. Engel, F. Würthner, *Chem. Eur. J.* **2007**, *13*, 436.
[18] P. Thissen, M. Valtiner, G. Grundmeier, *Langmuir* **2010**, *26*, 156.
[19] I. Levine, S. M. Weber, Y. Feldman, T. Bendikov, H. Cohen, D. Cahen, A. Vilan, *Langmuir* **2012**, *28*, 404.
[20] V. Marcon, D. W. Breiby, W. Pisula, J. Dahl, J. Kirkpatrick, S. Patwardhan, F. Grozema, D. Andrienko, *J. Am. Chem. Soc.* **2009**, *131*, 11426.
[21] F. Nolde, W. Pisula, S. Müller, C. Kohl, K. Müllen, *Chem. Mater.* **2006**, *18*, 3715.
[22] P. Kohn, L. Ghazaryan, G. Gupta, M. Sommer, A. Wicklein, M. Thelakkat, T. Thurn-Albrecht *Macromolecules* **2012**, *45*, 5676–5683.
[23] G. Klebe, F. Graser, E. Hadicke, J. Berndt, *Acta Cryst.* **1989**, *B45*, 69.
[24] M. R. Hansen, R. Graf, S. Sekharan, D. Sebastiani, *J. Am. Chem. Soc.* **2009**, *131*, 5251.
[25] O. Guillermet, M. Mossoyan-Déneux, M. Giorgi, A. Glachant, J. C. Mossoyan, *Thin Solid Films* **2006**, *514*, 25.
[26] A. Wicklein, A. Lang, M. Muth, M. Thelakkat, *J. Am. Chem. Soc.* **2009**, *131*, 14442.
[27] S. Fabiano, H. Wang, C. Piliego, C. Jaye, D. A. Fischer, Z. Chen, B. Pignataro, A. Facchetti, Y. L. Loo, M. A. Loi, *Adv. Funct. Mater.* **2011**, *21*, 4478.
[28] E. J. Meijer, G. H. Gelinck, E. van Veenendaal, B. H. Huisman, D. M. de Leeuw, T. M. Klapwijk, *Appl. Phys. Lett.* **2003**, *82*, 4576.
[29] G. Gelinck, P. Heremans, K. Nomoto, T. D. Anthopoulos, *Adv. Mater.* **2010**, *22*, 3778.
[30] M. Spijkman, E. C. P. Smits, P. W. M. Blom, D. M. de Leeuw, Y. Bon Saint Come, S. Setayesh, E. Cantatore, *Appl. Phys. Lett.* **2008**, *92*, 143304.
[31] A. Wicklein, A. Lang, M. Muth, M. Thelakkat, *J. Am. Chem. Soc.* **2009**, *131*, 14442.